ELSEVIER

Geomorphology 42 (2002) 1–24

GEOMORPHOLOGY

www.elsevier.com/locate/geomorph

# Glacial erosion and relief production in the Eastern Sierra Nevada, California

Simon H. Brocklehurst *, Kelin X. Whipple

*Department of Earth, Atmospheric and Planetary Sciences, Massachusetts Institute of Technology, Cambridge, MA 02139-4307, USA*

Received 22 May 2000; received in revised form 8 March 2001; accepted 9 March 2001

**Abstract**

The proposal that climate change can drive the uplift of mountain summits hinges on the requirement that glacial erosion significantly enhances the relief of a previously fluvially sculpted mountain range. We have tested this hypothesis through a systematic investigation of neighbouring glaciated and nonglaciated drainage basins on the eastern side of the Sierra Nevada, CA. We present a simple, objective method for investigating the relief structure of a drainage basin, which shows noticeable differences in the spatial distribution of relief between nonglaciated and glaciated basins. Glaciated basins on the eastern side of the Sierra Nevada have only ~80 m greater mean geophysical relief than nonglaciated basins. This "extra" relief, though, is attributable principally to the larger size of the glaciated basins, as geophysical relief generally increases with basin size. The glaciers on this side of the range were only responsible for relief production if they substantially increased headward erosion rates into low relief topography, such as an elevated plateau, and thus enlarged previously fluvial basins. We carried out a preliminary morphometric analysis to elucidate the importance of this effect and found that the glaciers of the eastern Sierra Nevada may have eroded headward at considerably faster rates than rivers, but only when they were not obstructed from doing so by either competing larger glaciers in adjacent valleys or transfluent ice at the head of the basin. Our results also suggest that, in temperate regions, alpine glaciers are capable of eroding downward at faster rates than rivers above the equilibrium line altitude (ELA). Although we can rule out significant peak uplift in response to local relief production, in the special case of the Sierra Nevada the concentration of mass removal above the ELA could have contributed to flexural uplift at the edge of a tilting block. © 2002 Elsevier Science B.V. All rights reserved.

*Keywords:* Glacial erosion; Relief; Landscape evolution

## 1. Introduction

The evolution of topography in a mountain range results from a complex interaction between tectonic forces, climatically driven erosion, and the geodynamic response to erosion. To understand the role of late Cenozoic climatic cooling in this system, it is necessary to evaluate the impact of glacial erosion on topography. How does landscape form evolve during glaciation of a previously fluvially sculpted landscape?

Modern topography documents that glaciated landscapes have a distinctive form, exhibiting cirques, arêtes, horns, hanging valleys, truncated spurs,

* Corresponding author. Fax: +1-617-252-1800.
*E-mail address:* shb@mit.edu (S.H. Brocklehurst).

0169-555X/02/$ - see front matter © 2002 Elsevier Science B.V. All rights reserved.
PII: S0169-555X(01)00069-1

and U-shaped flat-bottomed troughs (Fig. 1) (e.g., Sugden and John, 1976). The change in "missing mass," or "geophysical relief" (Small and Anderson, 1998), governs the local isostatic response to erosion. Net removal of mass, if concentrated geographically, will affect far-field flexural uplift (Small and Anderson, 1995). Geophysical relief can increase (and thus induce isostatic uplift) either if the erosion of summits and ridgelines is slower than mean erosion rates (i.e., valleys are growing deeper and/or wider; Fig. 2) or if incising drainage basins are enlarged at the expense of low relief topography. Does the development of the distinctive glaciated landscape result in a major change in relief structure? Small and Anderson (1995) proposed that a significant component of the late Cenozoic rock uplift in the Sierra Nevada was driven by the lithospheric response to coupled erosion of the Sierra Nevada and deposition in the adjacent Central Valley. Did climate change and development of glaciers in the Sierra Nevada contribute to this effect?

Landscape evolution models are being used increasingly to investigate linkages between surface and geodynamic processes, but cannot yet answer these questions. Most models treat only fluvial erosion and hillslope processes (e.g., Koons, 1989; Beaumont et al., 1992; Tucker and Slingerland, 1994, 1997). Furthermore, while much work has been focused on small-scale observations of glacial erosion processes (e.g., Boulton, 1974; Hallet, 1996), we do not have a good, quantitative understanding of the mesoscale effects of glacial erosion. Preliminary efforts at modelling mesoscale glacial erosion are currently underway (e.g., Braun et al., 1999; MacGregor et al., 2000; Merrand and Hallet, 2000; Tomkin and Braun, 2000).

The idea that mountain building processes and climate change are strongly coupled was first suggested by Chamberlin (1899). Raymo and Ruddiman (1992) built on his ideas, proposing that the tectonic uplift of mountain belts and elevated plateaux results in enhanced chemical erosion rates (drawing down atmospheric $CO_2$), an increase in albedo, and significant changes in atmospheric circulation. These three effects would combine to cause global cooling. The implication is that tectonic processes are the primary control on mountain range elevations. Wager (1933), on the other hand, suggested that an isostatic response to erosion at the edge of the Tibetan Plateau could explain the elevations of the Himalayas. Molnar and England (1990) further suggested that the transition to an icehouse climate state, driven by a non-tectonic mechanism, causes significant glacial erosion and relief production. The authors envisioned a positive

Fig. 1. View looking west up Shepherd Creek, showing fluvial reach downstream of a heavily glaciated upper valley, with a notable hanging valley on the south side, below Mount Williamson (far left). Notice the flatter valley floors in the glacial sections.

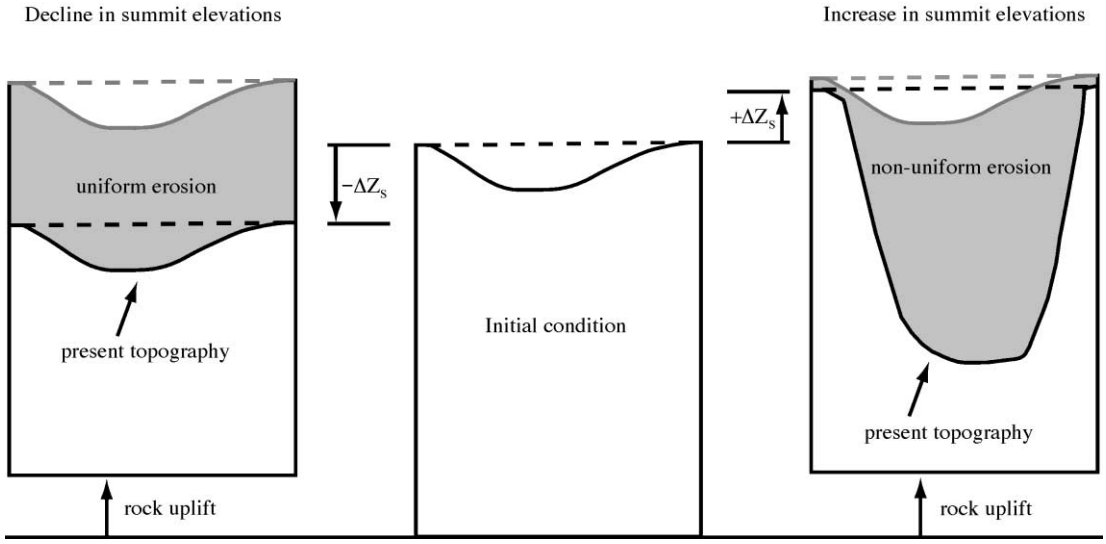


Fig. 2. Two cases of mountain erosion. Centre panel represents initial condition. The geophysical relief is the mean elevation difference between a smooth surface connecting the highest points in the landscape [dashed line—current (black) and prior (grey)] and the topography. When erosion (shaded area) is spatially uniform (left panel), there is no change in geophysical relief, and the sum of erosionally driven rock uplift and summit erosion results in lower summit elevations ($-\Delta Z_s$). When erosion is spatially variable (right panel), there is a notable increase in geophysical relief, and changes in summit elevation are positive ($+\Delta Z_s$) because rock uplift is greater than summit erosion. Rock uplift is the same in each case because average erosion, which drives rock uplift, is equal (shaded areas are the same size) (after Small and Anderson, 1998).

feedback between valley glacier erosion and rising summit and ridge elevations whereby the increased peak elevations resulting from isostatic adjustment enhance the mass balance of glaciers, increasing valley erosion and producing additional increases in elevation. Thus, peak uplift attributed to tectonic processes by earlier workers could instead be a result of relief production and subsequent isostatic peak uplift.

The limiting case of the isostatic response to fluvial incision of an initial plateau surface can account for 20–30% of peak uplift (Gilchrist et al., 1994; Montgomery, 1994), but this number decreases dramatically (~5%) if a realistic flexural strength for the lithosphere is considered (Montgomery, 1994). The more general case of enhanced fluvial erosion in a narrow fluvially sculpted mountain belt was examined by Whipple et al. (1999), who concluded that in almost all nonglacial landscapes an increase in the erosivity of the fluvial system would lead to a reduction in both trunk stream and tributary relief. Furthermore, such a change in climate cannot significantly increase the hillslope component of relief in a tectonically active orogen.

Turning to the glacial system, a first-order, unresolved question is whether glaciers can erode faster than bedrock streams. Hicks et al. (1990) used sediment yields in the Southern Alps of New Zealand to challenge the long-held view that glaciers are the more effective erosive agents. Hallet et al. (1996) used a global dataset to argue that glaciers are capable of eroding at significantly faster rates than rivers. Hallet et al. (2000) recently reduced the highest glacial erosion rate estimates from Alaska to ~10–60 mm/year, but these still exceed fluvial erosion rates. Brozović et al. (1997) suggested that their topographic analyses from the northwestern Himalaya showed that glacial erosion rates at high elevations can match the highest tectonic uplift rates, limiting regional-scale elevations to some distance above the equilibrium line altitude (ELA).

If glaciers are more efficient erosive agents, are they able to produce relief? Small and Anderson

(1998) demonstrated that differential erosion rates occurred between the summit flats and valley floors in the glaciated Wind River Range, Wyoming, but that the resulting relief production yielded negligible peak uplift, especially when the flexural strength of the crust was considered. Whipple et al. (1999) presented the following theoretical argument illustrating why relief production in the glacial system is probably limited to a few hundred metres in most cases. Extra relief due to ice-buttressing of rock slopes or the development of a U-shaped valley cross-section depends on ice thickness, while relief due to hanging valleys depends on the difference in ice thickness between tributaries and the trunk stream. MacGregor et al.'s (2000) modelling study confirmed that hanging valley relief is caused by both ponding of tributary ice against the trunk stream ice and the difference between tributary and trunk stream ice discharge. In most temperate alpine settings, ice thicknesses and tributary-trunk stream ice thickness differences are limited to a few hundred metres. Exceptional glaciers in the Swiss Alps or Himalayas might have reached a kilometre in thickness during the Pleistocene.

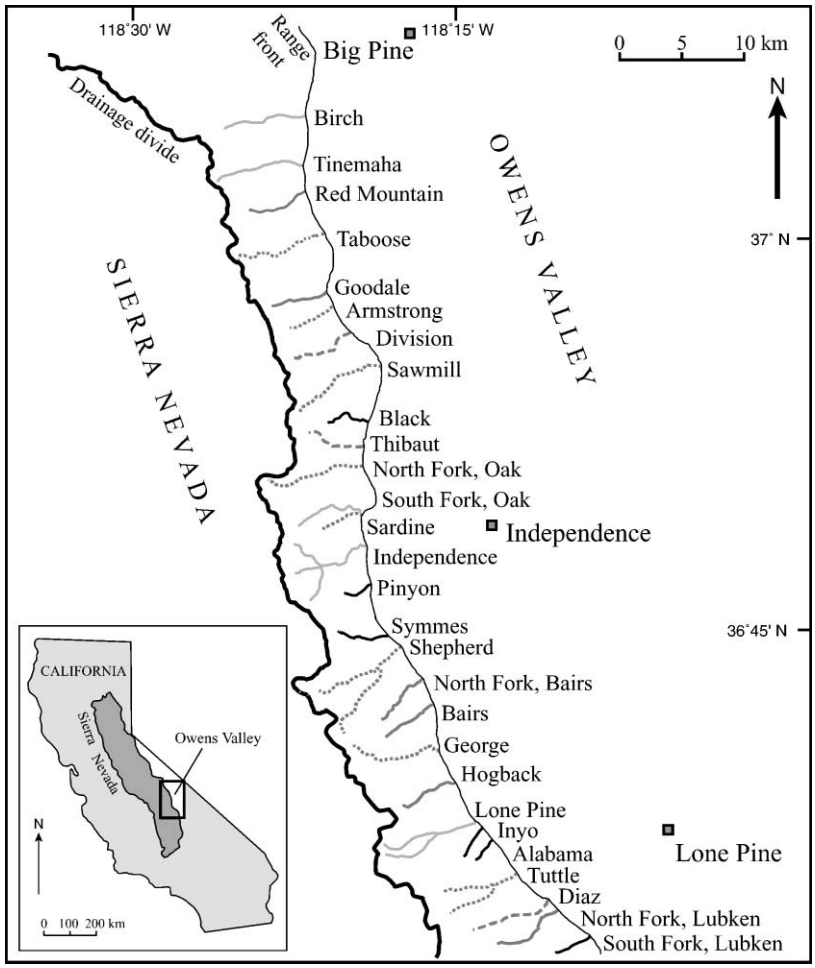


Fig. 3. Study site on the eastern side of the Sierra Nevada, California, highlighted on the inset map. Our five categories of basin, based on the degree of glaciation at the Last Glacial Maximum, are illustrated as follows: nonglaciated (black), minor glaciation (medium grey, dashed), moderate glaciation (medium grey, solid), significant glaciation (medium grey, dotted), and full glaciation (light grey).

Given that climate change and glacial erosion have variously been proposed to raise, have negligible effect on, or lower peak elevations, while probably increasing relief, but by an undetermined amount, clarification of the effect of glacial erosion on the landscape is clearly needed. Two critical questions are (i) how does glacial erosion impact range crest elevations? and (ii) how does glacial erosion impact the relief structure of the landscape?

The aim of this study was to address these questions through a careful comparison of nonglaciated and glaciated topography. A study of the eastern Sierra Nevada, between the towns of Lone Pine and Big Pine (Fig. 3), was undertaken (i) to determine whether glacial erosion has a significant impact on range crest elevations, (ii) to quantify the impact of glaciation on geophysical relief, and (iii) to assess whether glacial erosion has made an important contribution to erosional unloading (Small and Anderson, 1995). In this study area, adjacent drainage basins encompass the full spectrum from those that were completely unglaciated to those that were fully occupied by glacial ice during the Last Glacial Maximum (LGM). (While we realise that all of our drainage basins have experienced climatic cooling events (''glaciations''), we use the term glaciation to refer to the development of a glacier within a given drainage basin.) This allowed a direct comparison of the topography and relief structure between the two endmember cases, no glaciation and full glaciation, while the range of extents of glaciation permitted us to look at intermediate cases. Thus, we could effect a systematic evaluation of the consequences of glacial erosion on a previously fluvially sculpted mountain range in a temperate region without dramatic tectonic activity. In the current absence of glacial ice from the study area, the landforms produced by glaciation are exposed and readily analysed.

The core component of this study was the development of a novel and simple approach to calculate relief on a basin-wide scale, using the freely available US Geological Survey (USGS) 30-m resolution digital elevation models (DEMs). We compared the relief in glaciated and nonglaciated drainage basins and used the nonglaciated basins to constrain a fluvial erosion model. The model was used to estimate nonglacial topography both (i) along the longitudinal profile and (ii) for the basin as a whole, to suggest how the glaciated basins might look now had ice never occupied these basins.

## 2. Field site

We studied 28 individual drainage basins (Fig. 3) that have experienced similar tectonic and climatic histories. Present-day tectonic activity is dominated by strike-slip motion on the Owens Valley Fault farther to the east, although the range front normal fault may still be active, contributing to minor uplift rates ($\sim$0.2 mm/year; Gillespie, 1982). On a regional scale, this section of the Sierra Nevada comprises homogeneous Cretaceous granodiorites and quartz monzonites (Moore, 1963, 1981; Bateman, 1965). Triassic, Jurassic, and Paleozoic metamorphic rocks are minor components. Hence, major topographic differences between the drainage basins can be attributed principally to different glaciation histories. This region has seen a number of previous glacial studies (e.g., Gillespie, 1982; Burbank, 1991; Clark et al., 1994; Clark and Gillespie, 1997). However, this is the first quantitative analysis of the mesoscale impact of glacial erosion in this area.

A flow routing routine in ArcInfo was used to extract the drainage network structures of each of the basins from USGS 30-m DEMs (Table 1). The downstream extent of each drainage basin was taken to coincide with the range front, so as to exclude the alluvial fan regime and allow reasonable and consistent comparison between basins. The drainages were divided into five categories on the basis of the degree of glaciation experienced at the LGM: none, minor, moderate, significant, and full. We used LGM ice extents from aerial photograph interpretation, field observations, and previous mapping (e.g., Gillespie, 1982) as a proxy for relative ice extent throughout the Quaternary, although we appreciate that these do not represent the average ice extents during the Quaternary (Porter, 1989). ''Full glaciation'' symbolises LGM glaciers extending to the range front, while minor, moderate, and significant glaciers extended $\sim$1/4, $\sim$1/2, and $\sim$3/4 of the length of the drainage basin, respectively. The three middle categories were also considered collectively as ''partial glaciation.''

Table 1
Summary of topographic characteristics

| Basin | Degree of glaciation | Length (km) | Headwall elevation (m) | Drainage area ($km^2$) | Longitudinal profile | | | Basin-wide | | |
|---|---|---|---|---|---|---|---|---|---|---|
| | | | | | $\theta$ | $\ln(k_s)$ (fixed $\theta$) | $S_r$ ($A_r=10^6$ $m^2$) | $\theta$ | $\ln(k_s)$ (fixed $\theta$) | $S_r$ ($A_r=10^6$ $m^2$) |
| Alabama | None | 4.31 | 3738 | 3.15 | 0.32±0.07 | 3.38±1.60 | 0.378 | 0.23±0.04 | 2.88±0.48 | 0.413 |
| Black | None | 5.47 | 3564 | 6.88 | 0.20±0.07 | 3.49±1.67 | 0.389 | 0.19±0.06 | 2.76±0.73 | 0.368 |
| Inyo | None | 3.98 | 3901 | 2.93 | 0.37±0.06 | 3.41±1.59 | 0.391 | 0.27±0.06 | 2.87±0.80 | 0.409 |
| Pinyon | None | 7.37 | 3753 | 12.6 | 0.19±0.06 | 3.41±1.72 | 0.337 | 0.23±0.04 | 2.76±0.54 | 0.363 |
| South Fork, Lubken | None | 3.43 | 3194 | 3.41 | 0.45±0.08 | 3.34±1.57 | 0.357 | 0.38±0.07 | 2.67±0.83 | 0.313 |
| Symmes | None | 6.54 | 3963 | 11.8 | 0.37±0.05 | 3.32±1.68 | 0.374 | 0.29±0.03 | 2.72±0.36 | 0.352 |
| Diaz | Minor | 8.67 | 4092 | 11.4 | −0.01±0.05 | 3.38±1.73 | 0.251 | 0.17±0.07 | 2.52±0.91 | 0.281 |
| Division | Minor | 6.39 | 3747 | 12.8 | 0.04±0.05 | 3.44±1.71 | 0.299 | 0.08±0.07 | 2.41±0.87 | 0.258 |
| Thibaut | Minor | 7.88 | 3826 | 8.74 | 0.00±0.07 | 3.40±1.67 | 0.303 | 0.24±0.06 | 2.62±0.86 | 0.318 |
| Bairs | Moderate | 6.94 | 3944 | 7.71 | 0.13±0.05 | 3.33±1.67 | 0.313 | 0.18±0.04 | 2.69±0.53 | 0.339 |
| Goodale | Moderate | 13.27 | 4034 | 20.8 | 0.12±0.06 | 3.55±1.76 | 0.333 | 0.07±0.05 | 2.64±0.62 | 0.316 |
| Hogback | Moderate | 5.76 | 3955 | 12.4 | 0.14±0.07 | 3.47±1.69 | 0.352 | 0.26±0.07 | 2.66±0.96 | 0.331 |
| North Fork, Bairs | Moderate | 8.44 | 4330 | 10.0 | 0.20±0.05 | 3.36±1.68 | 0.336 | 0.22±0.04 | 2.69±0.60 | 0.339 |
| North Fork, Lubken | Moderate | 7.54 | 3854 | 10.1 | 0.19±0.07 | 3.43±1.71 | 0.345 | 0.20±0.04 | 2.65±0.59 | 0.322 |
| Red Mountain | Moderate | 8.13 | 4064 | 16.9 | 0.05±0.05 | 3.36±1.74 | 0.261 | 0.15±0.05 | 2.55±0.73 | 0.286 |
| Armstrong | Significant | 6.72 | 3616 | 8.17 | 0.08±0.07 | 3.29±1.72 | 0.267 | 0.13±0.06 | 2.23±0.78 | 0.215 |
| George | Significant | 11.37 | 4105 | 24.9 | 0.16±0.04 | 3.45±1.80 | 0.297 | 0.15±0.03 | 2.66±0.38 | 0.314 |
| North Fork, Oak | Significant | 10.41 | 4016 | 20.9 | 0.13±0.05 | 3.39±1.80 | 0.267 | 0.14±0.04 | 2.49±0.62 | 0.261 |
| Sardine | Significant | 5.63 | 3835 | 5.16 | −0.10±0.07 | 3.46±1.67 | 0.302 | 0.05±0.09 | 2.57±1.23 | 0.321 |
| Sawmill | Significant | 12.02 | 3968 | 19.6 | 0.00±0.05 | 3.48±1.80 | 0.232 | 0.20±0.08 | 2.19±1.15 | 0.202 |
| Shepherd | Significant | 16.38 | 3988 | 36.0 | 0.08±0.05 | 3.33±1.80 | 0.233 | 0.24±0.03 | 2.54±0.39 | 0.285 |
| Taboose | Significant | 10.67 | 3846 | 19.1 | 0.07±0.06 | 3.42±1.81 | 0.243 | 0.20±0.04 | 2.67±0.48 | 0.331 |
| Tuttle | Significant | 9.25 | 4096 | 21.6 | 0.08±0.06 | 3.33±1.77 | 0.242 | 0.21±0.02 | 2.71±0.28 | 0.343 |
| Birch | Full | 8.82 | 4036 | 13.4 | 0.09±0.05 | 3.34±1.77 | 0.251 | 0.23±0.06 | 2.40±0.86 | 0.250 |
| Independence | Full | 12.03 | 3955 | 30.4 | 0.13±0.05 | 3.43±1.78 | 0.293 | 0.20±0.07 | 2.26±0.98 | 0.213 |
| Lone Pine | Full | 10.86 | 4226 | 31.6 | 0.07±0.06 | 3.49±1.82 | 0.261 | 0.14±0.07 | 2.42±0.93 | 0.243 |
| South Fork, Oak | Full | 6.76 | 3951 | 10.0 | −0.03±0.06 | 3.35±1.74 | 0.230 | 0.14±0.10 | 2.35±1.34 | 0.243 |
| Tinemaha | Full | 8.72 | 4064 | 14.9 | 0.01±0.05 | 3.47±1.77 | 0.252 | 0.09±0.05 | 2.56±0.65 | 0.293 |
| Means | None | 5.18 | 3686 | 6.79 | 0.315±0.114 | 3.38±1.62 | 0.371 | 0.273±0.077 | 2.77±0.66 | 0.370 |
| | Partial[a] | 9.15 | 3960 | 15.7 | 0.080±0.093 | 3.40±1.76 | 0.287 | 0.169±0.080 | *2.56±0.77* | 0.298 |
| | *Minor* | *7.65* | *3888* | *11.0* | *0.012±0.048* | *3.41±1.74* | *0.284* | *0.163±0.089* | *2.54±0.90* | *0.286* |
| | *Moderate* | *8.35* | *4030* | *13.0* | *0.138±0.090* | *3.40±1.73* | *0.323* | *0.179±0.077* | *2.64±0.68* | *0.322* |
| | *Significant* | *10.31* | *3934* | *19.4* | *0.062±0.094* | *3.39±1.79* | *0.260* | *0.163±0.078* | *2.50±0.77* | *0.284* |
| | Full | 9.44 | 4046 | 20.1 | 0.079±0.081 | 3.37±1.82 | 0.258 | 0.160±0.085 | 2.38±0.99 | 0.249 |

[a] Figures for the three subdivisions of the 'Partial Glaciation' category are shown in italics.

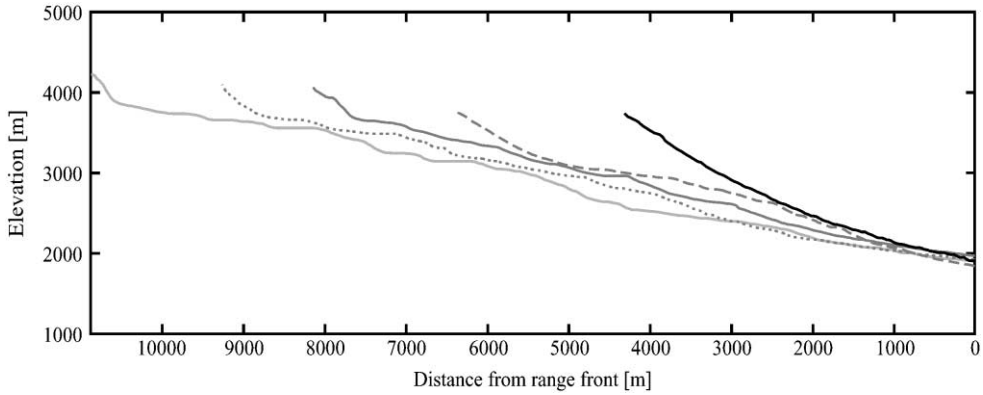


Fig. 4. Longitudinal profiles from Alabama Creek (nonglaciated, black), Division Creek (minor glaciation, medium grey, dashed), Red Mountain Creek (moderate glaciation, medium grey, solid), Tuttle Creek (significant glaciation, medium grey, dotted) and Lone Pine Creek (full glaciation, light grey). "Alabama Creek" is the name given to an unnamed creek that drains towards the Alabama Hills.

Some representative examples of longitudinal profiles taken from the five different categories of basin are shown in Fig. 4. The longitudinal profiles of the fluvial basins look much like those seen in other entirely unglaciated ranges (e.g., the Appalachians of Virginia and Maryland (Hack, 1957; Leopold et al., 1964), the King Range, northern California (Snyder et al., 2000)). Partial glaciation is typified by a flatter section in the upper reaches of the profile, while the lower parts retain the shape of a bedrock stream. Full glaciation yields stepped profiles with long, shallow sections separated by steeper steps, but the lower parts again resemble bedrock stream profiles.

## 3. Sub-ridgeline relief distribution

### 3.1. Method

Measurement of "relief" is a notoriously difficult problem, because in any landscape relief varies with the scale over which it is measured. Accordingly, many alternative definitions of relief are available.

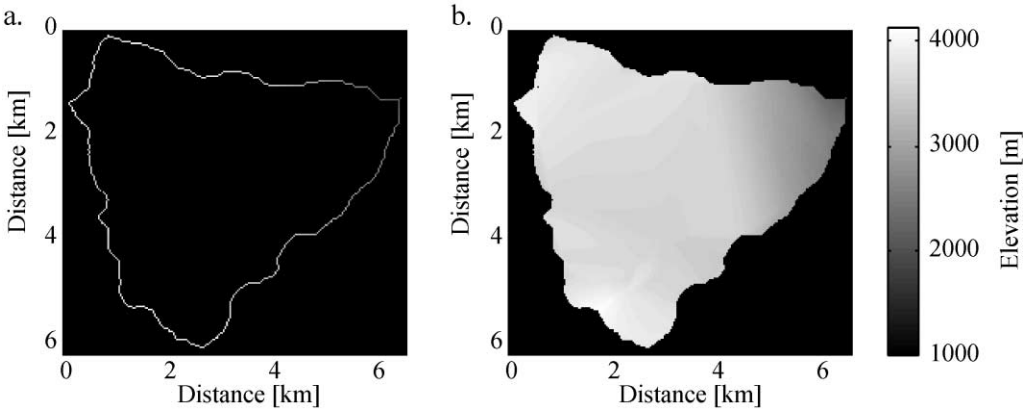


Fig. 5. Illustration of the "sub-ridgeline relief" method for Independence Creek. (a) Isolated ridgelines around the basin. (b) Interpolated smooth surface between these ridgelines.

At any given point, one can stand on the valley floor, pick a point on the ridgeline above, and call this difference in elevation the "relief." Relief can also be defined on the basis of differences in elevation between two points along a channel (the trunk stream or tributary relief, as appropriate), on a hillside (the hillslope relief) (e.g., Whipple et al., 1999), in an arbitrary direction (Weissel et al., 1994),

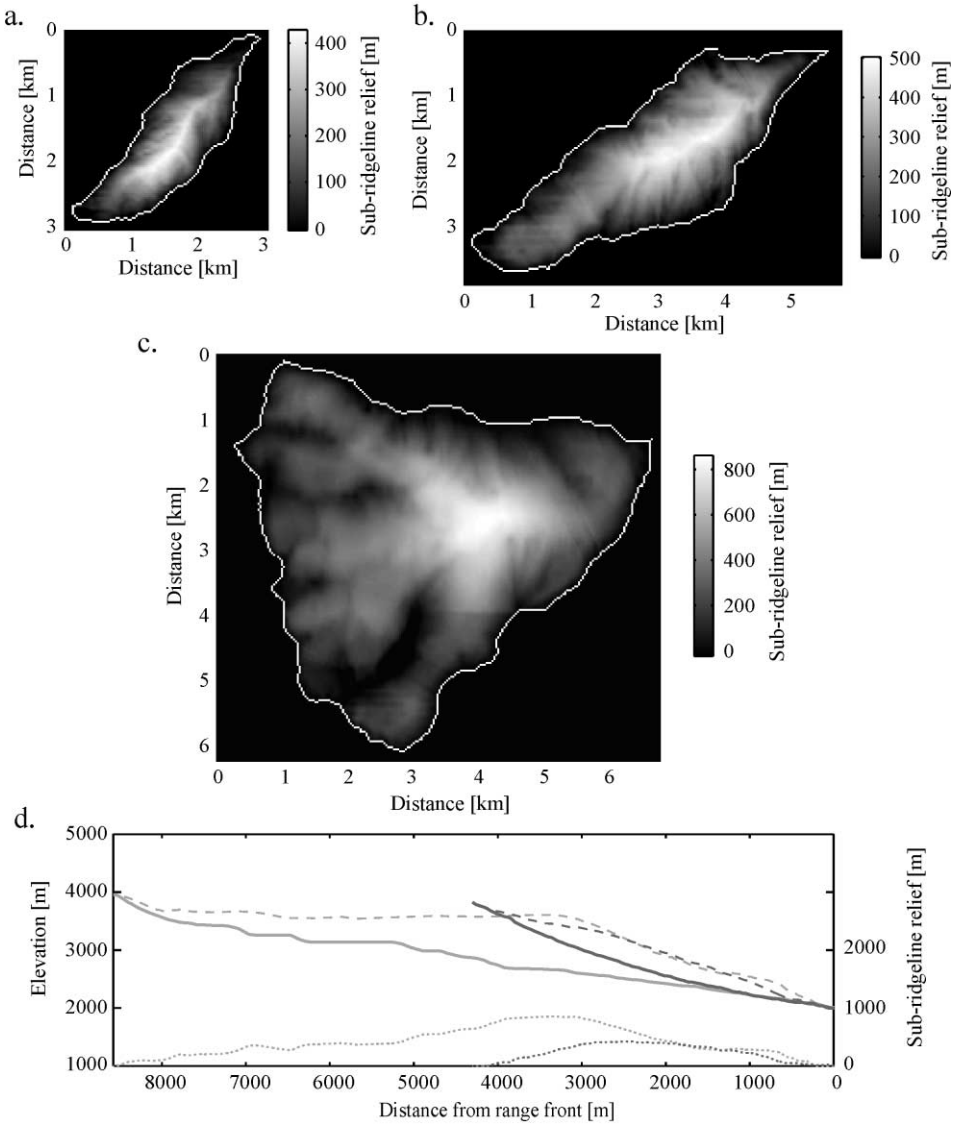


Fig. 6. Relief distribution for non-, partially, and fully glaciated valleys. In all cases, the basin outlet is on the right (east), and the scale is the same. (a) Relief distribution for the nonglaciated case, Alabama Creek, in map view. Notice the "bullseye" pattern of relief, greatest in the centre of the basin. (b) Relief distribution for the partially glaciated case, Bairs Creek, in map view. "Fingers" of high relief propagate upstream from high relief core. (c) Relief distribution for the fully glaciated case, Independence Creek, in map view. The high relief core shifts away from the range front in comparison with Alabama Creek. (d) Relief distribution along the longitudinal profiles of Alabama (dark grey) and Independence (light grey) Creeks. Solid lines are DEM topography, dashed lines are the sub-ridgeline interpolated surface along the longitudinal profile, and dotted lines are sub-ridgeline relief. Notice the flat ridgelines in the upper part of Independence Creek.

or within an arbitrary box (Ahnert, 1984). We define explicitly the nature of the "relief" that is relevant to our argument. For the purposes of a possible geodynamic response to erosion, the relevant measure is the geophysical relief (Small and Anderson, 1998). The geophysical relief is given by the volume of material "missing" below peaks and ridges divided by the surface area. These authors demonstrated that, if remnants of the pre-erosion surface are preserved, one can estimate not only the present relief but also the total amount and distribution of erosion. We have devised a similar, more general mathematical approach to measuring the modern geophysical relief structure to give a robust, objective, quantitative measure of the spatial distribution of relief (Brocklehurst and Whipple, 1999).

The first step in our method is to isolate the ridgelines outlining a given drainage basin (Fig. 5a). A cubic spline surface is then interpolated between these. The triangle-based cubic interpolation was found to be more satisfactory than either a triangle-based linear interpolation or a nearest-neighbour interpolation because it produces (i) a smooth surface and (ii) a surface that is continuous across the whole of the basin rather than producing a break down the centre line of the basin. We test whether any peaks or ridges within the basin protrude above this surface and repeat the interpolation with the surface also passing over these high points, to avoid underestimating the relief within the basin. This gives us a smooth reference datum (Fig. 5b) from which we subtract the current topography to give the spatial distribution of what we call "sub-ridgeline" relief (Fig. 6), i.e., the relief structure. In the absence of preserved remnants around the basin, we do not suggest that our interpolated surface represents the land surface at any time in the past, so we cannot equate our calculated sub-ridgeline relief with an amount of erosion. However, we can still compare the relief structures of different basins. Finally, we calculate the geophysical relief for each basin as the sub-ridgeline relief per unit area.

The isostatic response to relief production depends primarily on the isostatic response function, $i$ (Gilchrist et al., 1994):

$$i = \rho_c/\rho_m \quad (1)$$

where $\rho_c$ is the density of material eroded from the top of the crust, and $\rho_m$ is the density of the mantle at the depth of compensation. The value of $i$ gives the amount of isostatic uplift per unit depth of dissection and is generally slightly less than the mean geophysical relief ($\sim 0.82$ for typical crustal and mantle densities).

### 3.2. Results and interpretations

Our analyses revealed an apparent trend in the dependence of sub-ridgeline relief distribution on the degree of glaciation. Nonglaciated valleys exhibit a "bullseye" pattern of relief, greatest at the centre of the basin (Fig. 6a). Progressively greater glaciation first causes a propagation of high relief "fingers" up the valleys from the high relief core (Fig. 6b) and then an enlargement of this core (Fig. 6c). Fig. 6d illustrates the sub-ridgeline relief along the trunk streams of a nonglaciated and a glaciated basin along with the current longitudinal profiles and the elevations of our interpolated surfaces along these profiles. The maximum relief in the glaciated basin, Independence Creek, is greater than that in the nonglaciated basin, Alabama Creek, and is located farther from the range front. Geophysical relief in valleys experiencing minor, moderate, significant, and full glaciation is on average $\sim$17-m less, $\sim$28-, $\sim$60-, and $\sim$81-m greater than that in nonglaciated basins, respectively (Fig. 7). An increase in geophysical relief of $\sim$81 m would generate only $\sim$66 m of uplift in the extreme case of pure isostatic response to incision. This number would be reduced considerably for a realistic elastic thickness. Moreover, the apparent increase in relief with degree of glaciation could reflect principally the larger size of the glaciated basins. Accordingly, Fig. 7 also illustrates the geophysical relief in GOLEM fluvial simulations for each basin (see below), which in most cases is comparable with the geophysical relief from the DEM. We also undertook a series of simulations varying the size of a drainage basin of fixed shape. We used the shape, drainage network, and number of pixels (from the 30 m DEM) of Symmes Creek, but varied the pixel size between 10 and 55 m to generate the range of basin areas shown by the smooth curve on Fig. 7. This curve clearly demonstrates a trend of increasing geophysical relief with increasing drainage area, similar in magnitude to that seen comparing fluvial and glaciated basins.

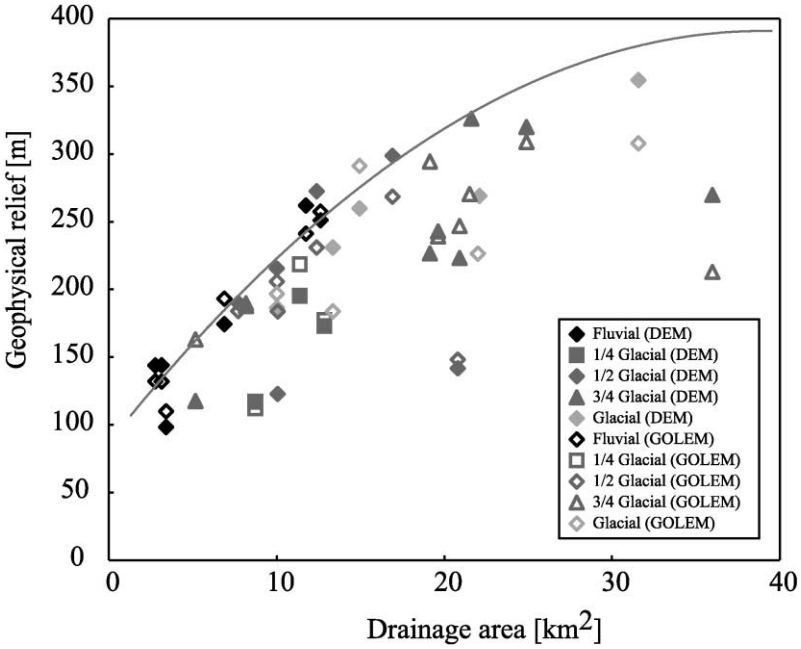


Fig. 7. Geophysical relief plotted against drainage area for current topography (DEM) and simulated topography (GOLEM), as explained in the text. The solid line represents simulating different-sized basins with the drainage pattern and basin shape of Symmes Creek (see text for explanation).

The interpolated surfaces used to define sub-ridgeline relief suggest that the ridgelines surrounding the glaciated basins are relatively flat for a significant proportion of the upper part of each basin (Fig. 6d). This is supported by the uniformity of headwall elevations, independent of basin size (Table 1). These observations can be interpreted as reflecting either prominent headward glacial erosion into a plateau surface, or significant lowering of hillslopes and ridgelines farther from the range front in response to downward cutting by the glaciers in the upper reaches of the glaciated basins. Simulations of nonglacial topography described below were used to evaluate the relative importance of these two possibilities.

## 4. Simulated nonglaciated topography

We simulated expected fluvial topography to address two questions: (i) how has glaciation changed the form of the landscape (and thus contributed to either isostatic or flexural uplift)? and (ii) are the observed differences in mean geophysical relief between the basins in the Sierra Nevada due purely to differences in drainage basin size (as suggested above)? Our approach was to use slope–drainage area analysis of the nonglaciated basins to constrain a model for bedrock channel erosion. This model was then employed with the drainage patterns of the glaciated basins to simulate the hypothetical modern forms of the basins should they never have been occupied by ice.

We focused first on the longitudinal profile because it is an important component of the relief structure (Whipple et al., 1999) and readily simulated. We used the error-weighted mean concavity and steepness from nonglaciated basins in concert with the present glacially influenced drainage structure to simulate a fluvial longitudinal profile for each glacially modified basin. As a simple indicator of likely changes to the longitudinal profile due to glaciation, we compared the current longitudinal profiles of glaciated basins with our simulations of expected present-day fluvial longitudinal profiles. We later suggest that this method can also be used as a tool to predict relative

headwall erosion rates. Moving to two-dimensional simulations allowed us to separate the effect of basin size from the effect of glaciation in the development of relief (Fig. 7). These simulations of expected fluvial topography, constrained by the drainage pattern and shape of a glaciated basin, also allowed us to address the question "what would the Sierra Nevada look like now if it had not been glaciated?" This was a question that we were unable to resolve on the basis of field studies alone, because insufficient evidence of the prior landform remains.

### 4.1. Slope–area analysis

Our simulations are based on the observed power–law relationship between slope and drainage area in fluvial topography (e.g., Flint, 1974), and thus require prior analysis of the slope–area data for the nonglaciated basins within the study area. Flint (1974) characterised fluvial topography in terms of two parameters: the concavity index, $\theta$, and the steepness index, $k_s$:

$$S = k_s A^{-\theta}. \quad (2)$$

We employed linear regression of the logarithms of local channel gradient, $S$, and drainage area, $A$, to determine the concavity and steepness in all of the basins. For the glaciated basins, this was purely for the purpose of comparison rather than to suggest a mechanistic interpretation of slope–area data for glacial erosion. The power–law relationship (Eq. (2)) is commonly observed in many fluvial systems (Flint, 1974; Tarboton et al., 1991; Montgomery and Foufoula-Georgiou, 1993; Willgoose, 1994; Snyder et al., 2000), and under the special conditions of steady state (erosion rate equal to uplift rate at all points) the concavity and steepness can be related to the parameters of the bedrock channel erosion model (e.g., Whipple and Tucker, 1999). The error-weighted mean concavities and steepnesses for the nonglaciated basins were employed in our subsequent fluvial simulations to generate topography with the same fundamental characteristics. Since we merely sought to reproduce similar topography, we did not need to assume that either the current fluvial topography or the simulated topography represent steady state conditions. The only assumption necessary is that the observed slope–area relationship for the nonglaciated basins (area $\sim 10$ km$^2$) can be extrapolated to the greater drainage area of the glaciated basins ($\sim 30$ km$^2$). Previous studies have demonstrated such a power–law relationship over larger ranges of drainage area (e.g., Tarboton et al., 1991; Whipple and Tucker, 1999).

The concavity and steepness were determined using two different sets of slope–area data: data along the trunk stream only, and data from the entire drainage basin. Restricting the analysis to the longitudinal profile of the trunk stream avoids complications due to errors in computing tributary flow paths across gently sloping terrain on ridges and valley floors and reduces scatter due to intra-basin variations. The stair-step nature of the DEM-derived nonglacial longitudinal profiles produces considerable scatter in slope–area data, but can be attributed to artefacts of DEM resolution and pit-filling routines. Smoothing of these data was achieved by calculating slopes on interpolated 10-m elevation contour intervals (Snyder et al., 2000). The same routine was employed with the glacial profiles, although glacial valleys naturally exhibit flat reaches, overdeepenings, and adverse slopes. The basin as a whole is the domain used by most previous workers (Tarboton et al., 1991; Montgomery and Foufoula-Georgiou, 1993; Willgoose, 1994; Tucker and Bras, 1998). For both analyses, we excluded the hillslopes above the channel heads from the regression, because the slope–area relation (Eq. (2)) is only applicable to the bedrock channel sections of the basin. We chose a critical drainage area for channel initiation of $10^5$ m$^2$, because it was at this area that there was a break in slope–area scaling in the majority of the basins, also discussed by Montgomery and Foufoula-Georgiou (1993) and Snyder et al. (2000). The slope distribution below this critical drainage area threshold gives representative slopes for the hillslope regions. By choosing the downstream extent of our basins to lie at the range front, we avoided areas with significant alluviation of the trunk stream and thus did not need to impose an upper limit on the drainage area considered in the regression analysis (see discussion in Snyder et al., 2000).

Nonglaciated basins are characterised by longitudinal profile concavities ($\theta$) with an error-weighted mean of $0.32 \pm 0.11$ ($1\sigma$) (Table 1). This figure

plunges dramatically to a mean of $0.08\pm0.09$ for partially glaciated basins and $0.07\pm0.08$ for fully glaciated basins. All of the glaciated basins have concavities that are significantly different from the nonglacial basins, but there is little variation between the four different categories of glacial extent. Clearly, one effect of glaciation is to reduce the overall concavity of the longitudinal profile. At drainage areas below the break in the slope–area relationship ($A<10^5$ m$^2$), the slopes cluster around 40°, so we take this as the maximum permitted hillslope angle in our subsequent simulations (see below).

Given the intimate relationship between concavity and steepness (derived from regression slope and intercept, respectively), we followed two different methods to determine meaningful measures of steepness. To obtain a representative $k_s$ for the nonglaciated basins for our subsequent modelling, we fixed the concavity at the error-weighted mean nonglaciated value and repeated the regressions for this subset of the basins (Snyder et al., 2000). To gain an indication of the errors on our determination of $k_s$, we also determined $k_s$ with the concavity fixed at the mean concavity plus and minus the $1\sigma$ error. For a concavity of 0.32, the mean value of $k_s$ for the nonglaciated basins is 30 ($\theta+1\sigma$: 149; $\theta-1\sigma$: 5.9). The errors in $k_s$ are not symmetrical as the steepness is the exponential of the intercept, which does have symmetrical errors. Where concavity varies considerably, the method employed by Snyder et al. (2000) is not ideal, so for the dataset as a whole we followed the technique suggested by Sklar and Dietrich (1998). Normalising by a representative area ($A_r$) in the centre of the range of drainage area data gives a representative slope, $S_r$, which expresses the relative steepness of the profile:

$$S = S_r(A/A_r)^{-\theta} \quad (3)$$

In our case $A_r$ was $10^6$ m$^2$. Fig. 8 shows that $S_r$ is not independent of concavity. The less concave, glaciated basins tend to also have lower representative slopes $S_r$, as suggested by Fig. 4. In other words, the glaciated basins are fundamentally less steep than their nonglaciated counterparts.

The basin-wide concavities average $0.27\pm0.08$ ($1\sigma$) for nonglaciated basins, $0.17\pm0.08$ for partially glaciated basins, and $0.16\pm0.08$ for fully glaciated basins (Table 1). Again, the subcategorisation of the

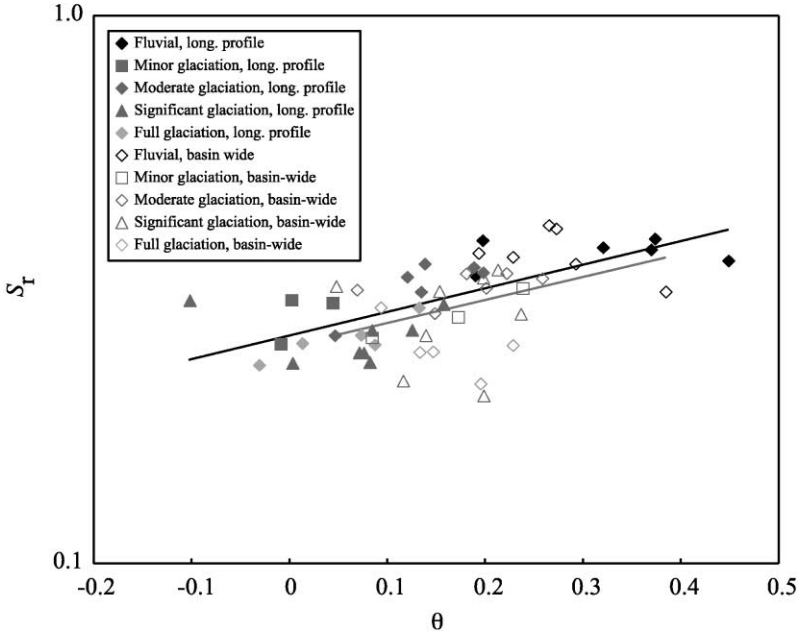


Fig. 8. Steepness index, $S_r$, plotted on a log scale against concavity, $\theta$, for both longitudinal profile and basin-wide data. The dark grey line is the best fit exponential for the longitudinal profile data, the pale grey line the best fit for the basin-wide data.

partially glaciated basins reveals little. A basin-wide concavity set at 0.27 yields a mean $k_s$ in the nonglaciated basins of 16 ($\theta+1\sigma$: 31; $\theta-1\sigma$: 8.3). In terms of steepness, the basin-wide data show a near identical pattern to that of the longitudinal profile data, with shallower representative slopes in the less concave glaciated basins (Fig. 8).

The longitudinal profile concavity is noticeably lower than the basin-wide concavity in the glaciated basins because of the low slopes in the upper reaches of the main channel in the glacial system, corresponding to the floors of cirques and overdeepenings. These low slopes act to decrease the concavity of the trunk stream profile as defined by the slope of the best-fit line in log slope–log area space. When the whole basin is considered, steeper slopes at low drainage areas in tributaries (especially near the range front) act against a decline in concavity. Such distinctive low slopes high in the glaciated drainage basins are also clearly demonstrated in the hypsometry and slope–elevation distributions of the eastern Sierra Nevada (Brocklehurst and Whipple, 1999, 2000). In the nonglacial basins, the longitudinal profile and basin-wide concavities are the same within error.

### 4.2. One-dimensional simulated topography

#### 4.2.1. Methods

The one-dimensional simulations were obtained by integrating the slope–area relation established for nonglaciated basins along the longitudinal profiles of the glaciated basins. We also analysed the nonglaciated basins to verify that we could reproduce a close approximation to the current topography using the mean values reported above. The concavity and steepness indices came from the longitudinal profile-restricted data (see above), with a maximum permitted hillslope angle at the channel head of 40°, also from our slope–area analyses. Simply integrating the observed relationship requires no assumptions about steady state for either the current nonglacial topography or our simulated fluvial topography. We fixed the outlet elevation at its current elevation, reasoning that the glacial system has had very little opportunity to modify this elevation by either erosion (very short ice residence time in this region even for the fully glaciated cases) or by deposition (the vast majority of sediment continues downstream to the alluvial fans and beyond). We obtained an indication of the accuracy of our simulated profiles by employing the mean concavity with the $1\sigma$ error either added or subtracted and the correspondingly adjusted steepnesses, as described above (dashed lines on Fig. 9).

#### 4.2.2. Results and interpretations

In our simple one-dimensional simulations, we were able to accurately reproduce a typical nonglaciated profile using the error-weighted mean and associated steepness (e.g., Alabama Creek, Fig. 9a). The mean concavity and steepness produced a more representative profile than either the upper- or lower-bound concavities with their corresponding steepnesses. We found that the glaciated basins fell into two categories. For some of the glaciated basins, we generated a very close match between the simulated profile and the present profile lower in the basin, but with considerable deviation in the upper part of the basin where the simulated profile lay at a much higher elevation (e.g., Birch Creek, Fig. 9b). In the remaining cases, the simulated fluvial profile lay significantly below the present topographic profile in the middle reaches (e.g., Tinemaha Creek, Fig. 9c). These "undercutting" profiles were found independently of the degree of glaciation.

Our interpretation of the deviation between simulated and observed topography in the upper part of non-undercutting glaciated basins is that considerable downcutting is required here to evolve from a typical nonglaciated profile to the currently observed glaciated profiles. Had the glaciers not developed and eroded a significant "extra" amount of material, the observed fluvial profiles would currently have a profile similar to our simulations. Thus, we suggest that at higher elevations in the Sierra Nevada glaciers erode faster than streams. The good agreement lower in the basin may be due to the short residence time of glaciers in this part of the basin, even in the fully glaciated cases (Porter, 1989), or might indicate that glacial erosion in the ablation zone of these glaciers was either inefficient or dominated by subglacial water.

One could interpret the undercutting profiles (Fig. 9c) as representing lower erosion rates in this part of the glacial system than would have occurred in the fluvial system. Alternatively, locally resistant bedrock

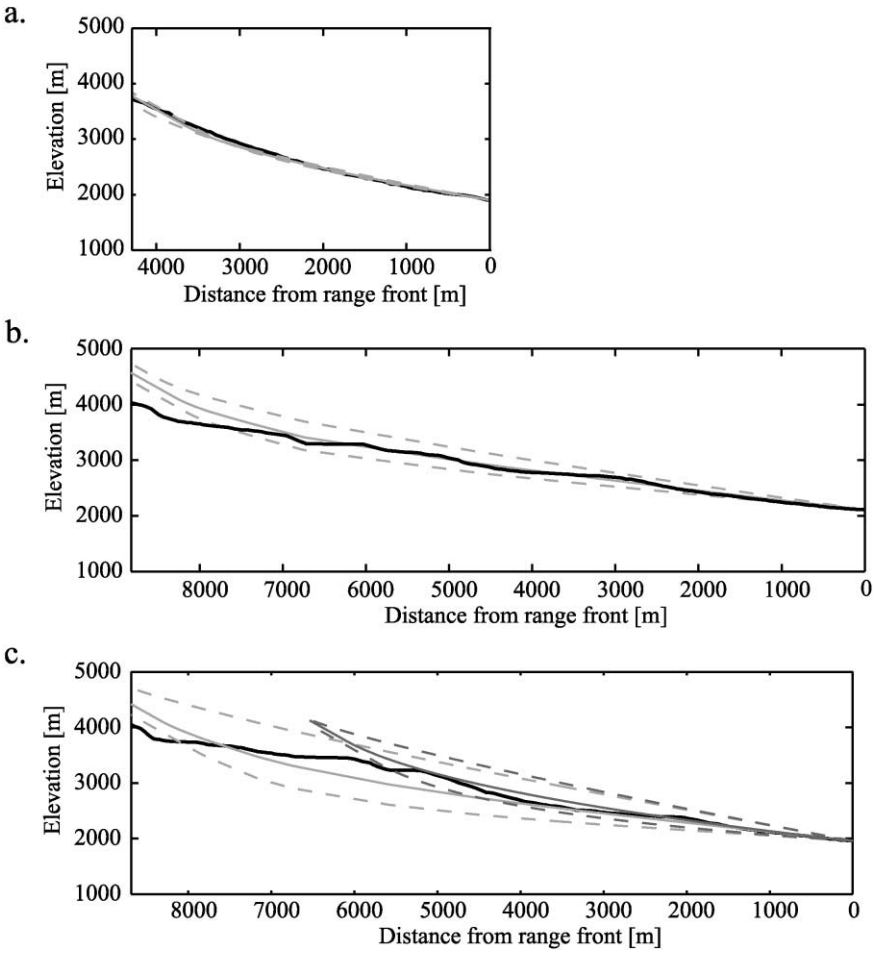


Fig. 9. (a) One-dimensional simulated profiles for Alabama Creek, a nonglaciated basin. The black line is the longitudinal profile extracted from the DEM, the pale grey, solid line is the simulated longitudinal profile, and the pale grey, dashed lines are the simulated longitudinal profiles varying concavity and steepness in concert by $\pm 1\sigma$. (b) Birch Creek. Key as for Alabama Creek. (c) Tinemaha Creek. Key as for Alabama Creek, plus the dark grey, solid line is the shortened, simulated longitudinal profile (see text), and the dark grey, dashed lines are the shortened, simulated longitudinal profiles, varying concavity and steepness by $\pm 1\sigma$.

might be responsible for the observed undercutting (observed profile not eroding as much as our simulation predicts). However, we note that in each case, shortening the simulated profile from the divide (upstream end) places it more in line with the observed topographic profile in the lower reaches of the basin. Hence, our preferred interpretation is that "undercutting" is a consequence of faster (horizontal) headwall erosion rates in the glacial system (as discussed below). That is, if glaciation had not occurred, some of the drainages on the eastern side of the Sierra Nevada would now be shorter.

### *4.3. Two-dimensional simulated topography (GOLEM)*

#### *4.3.1. Methods*

We employed the nonglaciated basin-wide error-weighted mean concavity and steepness statistics as the principle inputs to the Geologic–Orogenic Landscape Evolution Model (GOLEM, described in detail by Tucker and Slingerland, 1994, 1997) to simulate most likely present-day fluvial landforms. GOLEM simulates basin evolution under the action of tectonic uplift, weathering processes, hillslope transport, and

bedrock channel erosion and sediment transport. While this set of processes is not exhaustive, it incorporates the most important landscape-forming processes in basins that are dominated by physical rather than chemical erosion. Bedrock-channel erosion follows a shear-stress derived power–law relationship. We prescribed the basin outline and initial drainage pattern to be the same as for the current topography in order to allow meaningful comparison between the simulated and current topography. Our two-dimensional simulations have not addressed the possibility of headwall erosion directly. The model was run until it reached a steady-state condition, but this was done solely to reproduce the slope–area

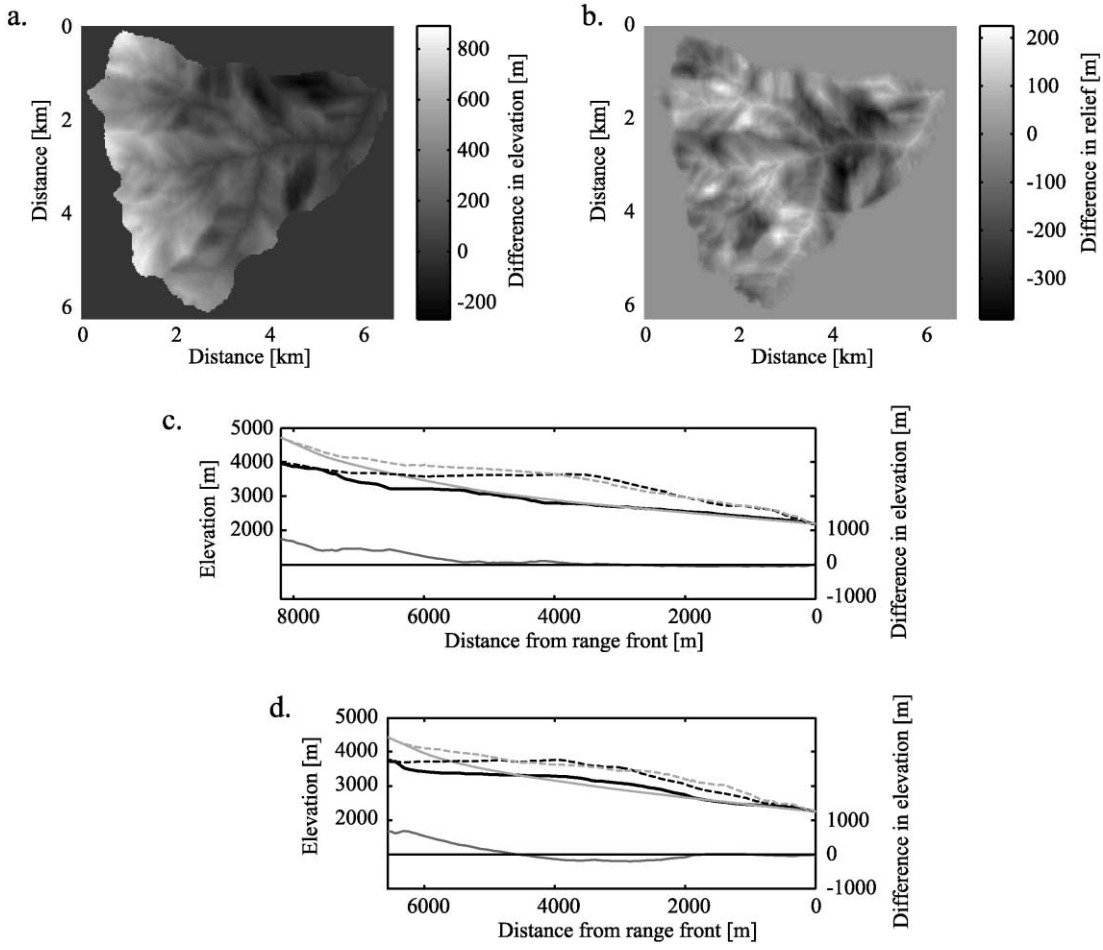


Fig. 10. Two-dimensional simulations of Independence Creek and South Fork, Oak Creek. (a) Present topography subtracted from the GOLEM simulated topography for Independence Creek, in map view (see text). Simulated topography is noticeably higher in the upper parts of the basin. (b) Present sub-ridgeline relief subtracted from GOLEM simulated sub-ridgeline relief for Independence Creek, in map view. Redistribution of relief comprises higher relief in the glacial system at high elevations and also in the lower U-shaped sections, but lower relief where the different tributaries come together. (c) Independence Creek. Longitudinal profiles drawn from the present topography (black) and simulated topography (pale grey) with the difference between the two in dark grey. Also shown are the interpolated ridgeline surfaces along the profiles (present topography—black, dashed; simulated topography—pale grey, dashed). Comparing the observed and simulated topography, both the valley floor and the ridgeline agree well at lower elevations and then diverge considerably higher up, with the simulated ridgeline and longitudinal profile considerably higher. (d) South Fork, Oak Creek. Key as for Independence Creek. The simulated profile undercuts the present topography in the middle reaches, suggesting headwall erosion in the glacial system (see text).

relation currently observed in nonglaciated basins, rather than to necessarily suggest the landscape now or in our simulations is in steady state. After seeing that the mean concavity and steepness produced the most realistic fluvial profiles in the one-dimensional case, we concentrated on these values here. Once the simulated topography had been generated, we calculated sub-ridgeline relief as before for comparison with relief in modern basins (Fig. 7) and to allow us to contrast ridgeline behaviour alongside any changes in the channels.

*4.3.2. Results and interpretation*

The GOLEM simulations accurately reproduced the modern topography in the nonglaciated basins, matching the topography of the basin and reproducing the total geophysical relief and its spatial distribution (Fig. 7). The simulations of glaciated basins revealed in more detail and in two dimensions the same patterns that were seen in our simple one-dimensional simulations (Fig. 10). In most cases, the simulated and present elevations are strikingly similar in the lower parts of the basin, but diverge noticeably in the upper part of the basin. Fig. 10a and c highlight that, in such instances, both ridgelines and valley floors are lower in the present topography. In other cases, the simulated topography undercuts the observed topography in the same way as in our one-dimensional cases (Fig. 10d). As before, the presence or absence of "undercutting" in the glaciated basins is independent of the degree of glaciation, and we attribute the undercutting to headwall erosion in the glacial system. Our calculation of sub-ridgeline relief shows that glaciation caused significant reorganisation of the relief structure, with greater relief at high elevations in the cirques, and reduced relief where tributaries come together lower in the basins in comparison with a simulated fluvial counterpart (Fig. 10b). The redistribution of relief is more pronounced the greater the degree of glaciation. However, our calculated geophysical relief is similar for the simulated fluvial topography and the current topography (Fig. 7). The only clear distinction between the two occurs in the fully glaciated basins, where geophysical relief is on average $\sim 25$ m greater using the observed topography (Fig. 7).

We attribute the differences in topography in the upper part of the basin in Fig. 10a to greater efficiency in downcutting at high elevations and/or headwall erosion (see below) by glaciers. Ridgelines could be lowered (Fig. 10c,d) either by periglacial ridgetop processes or through the mass wasting of hillslopes reacting to enhanced rates of downcutting by the valley glaciers. The redistribution of relief that is observed between simulated and observed topography indicates that glacial erosion mechanisms that both enhance and reduce relief have been active (Whipple et al., 1999), operating within the overall scheme of downward cutting at high elevations. The near-identical geophysical relief values in simulated and observed basins suggest that the major portion of the differences in relief between the current basins can be attributed to their sizes: nonglaciated and glaciated basins of the same size and shape have very similar relief. If our proposed headwall cutting incises an elevated plateau, the mean relief will be increased. However, if the topography is already dissected, the headwall cutting will act only to lower divides. In either case, this will be accompanied by lowering of valley floor, peak, and ridgeline elevations in the upper part of the basin.

## 5. Headwall erosion

As described above, both our one- and two-dimensional simulations led us to hypothesise that headwall erosion rates in the glacial system might exceed those in the fluvial system. Headwall erosion rates are not well understood in either the fluvial or glacial systems. We view this as a major unsolved problem in landscape evolution. A couple of mechanisms have been proposed to enhance headwall erosion rates in the glacial system. In the upper

Fig. 11. (a) Contour map of Tinemaha and Birch Creeks and the south fork of Big Pine Creek. Profiles plotted in (b)–(d) as illustrated. Notice the westward step in the divide at the head of Tinemaha Creek. (b) Tinemaha Creek, profile 1 (present topography—black; full-length simulation—medium grey; shortened simulation—pale grey; simulated longitudinal profiles varying concavity and steepness by $\pm 1\sigma$—dashed). Estimated headwall erosion: 500 m. (c) Tinemaha Creek, profile 2 (key as before). Estimated headwall erosion: 2150 m. (e) Tinemaha Creek, profile 3 (key as before). Estimated headwall erosion: 1400 m.

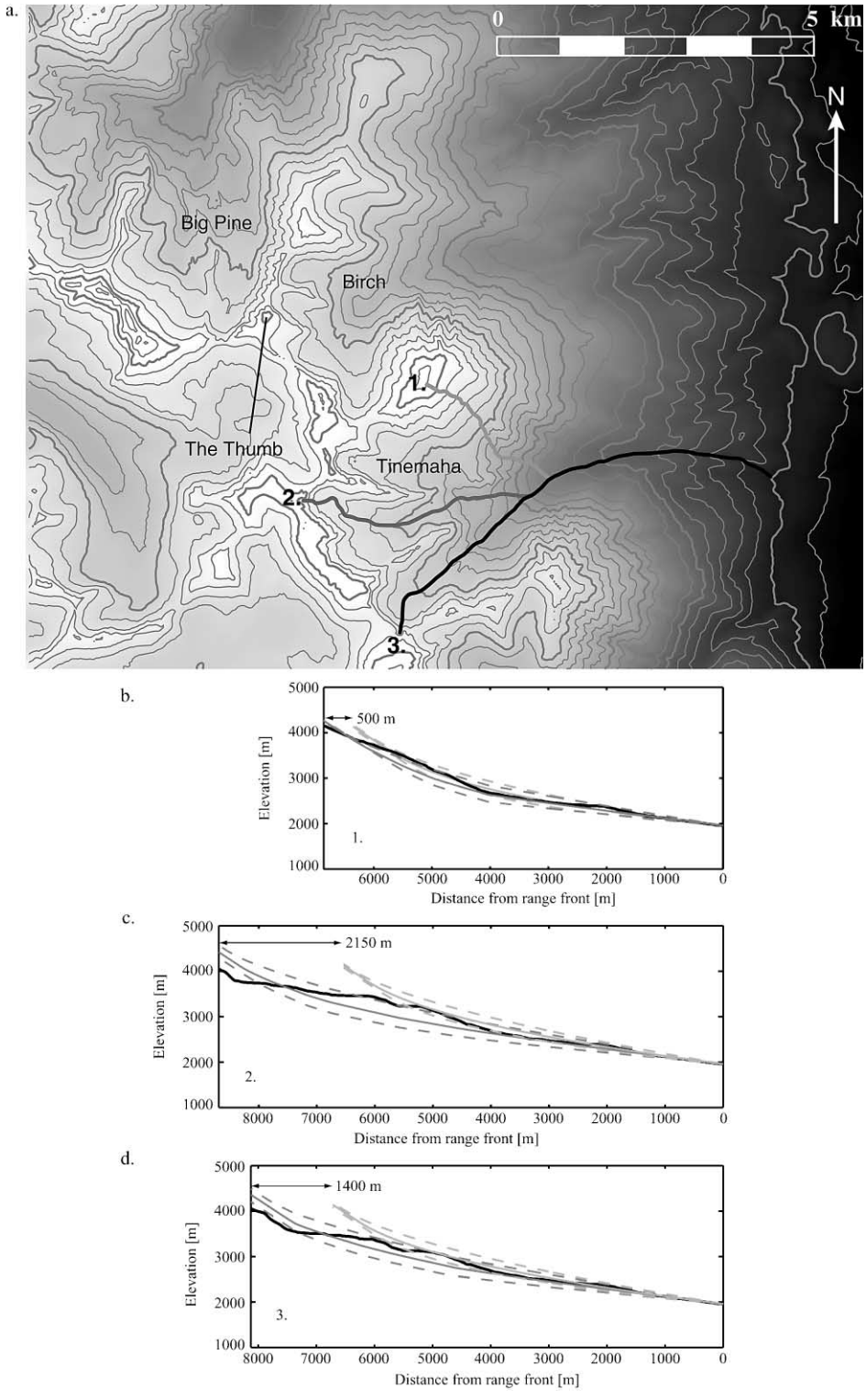
a.
0
5 km
N
Big Pine
Birch
1.
The Thumb
Tinemaha
2.
3.
b.
500 m
Elevation [m]
1.
Distance from range front [m]
c.
2150 m
Elevation [m]
2.
Distance from range front [m]
d.
1400 m
Elevation [m]
3.
Distance from range front [m]

headwall, freeze–thaw processes govern erosion rates. Matsuoka and Sakai (1999) linked observed rockfalls in the Japanese Alps to seasonal thawing. In the lower headwall, the bergschrund allows water to reach the glacier bed, causing large amplitude subglacial water-pressure fluctuations that may facilitate rapid erosion by quarrying (Hooke, 1991; Hallet, 1996; Alley et al., 1999).

As shown in Fig. 9c, where we represent faster glacial headwall erosion with a simulated fluvial profile constructed for a shorter, reduced area basin, we can obtain a good fit between observed and

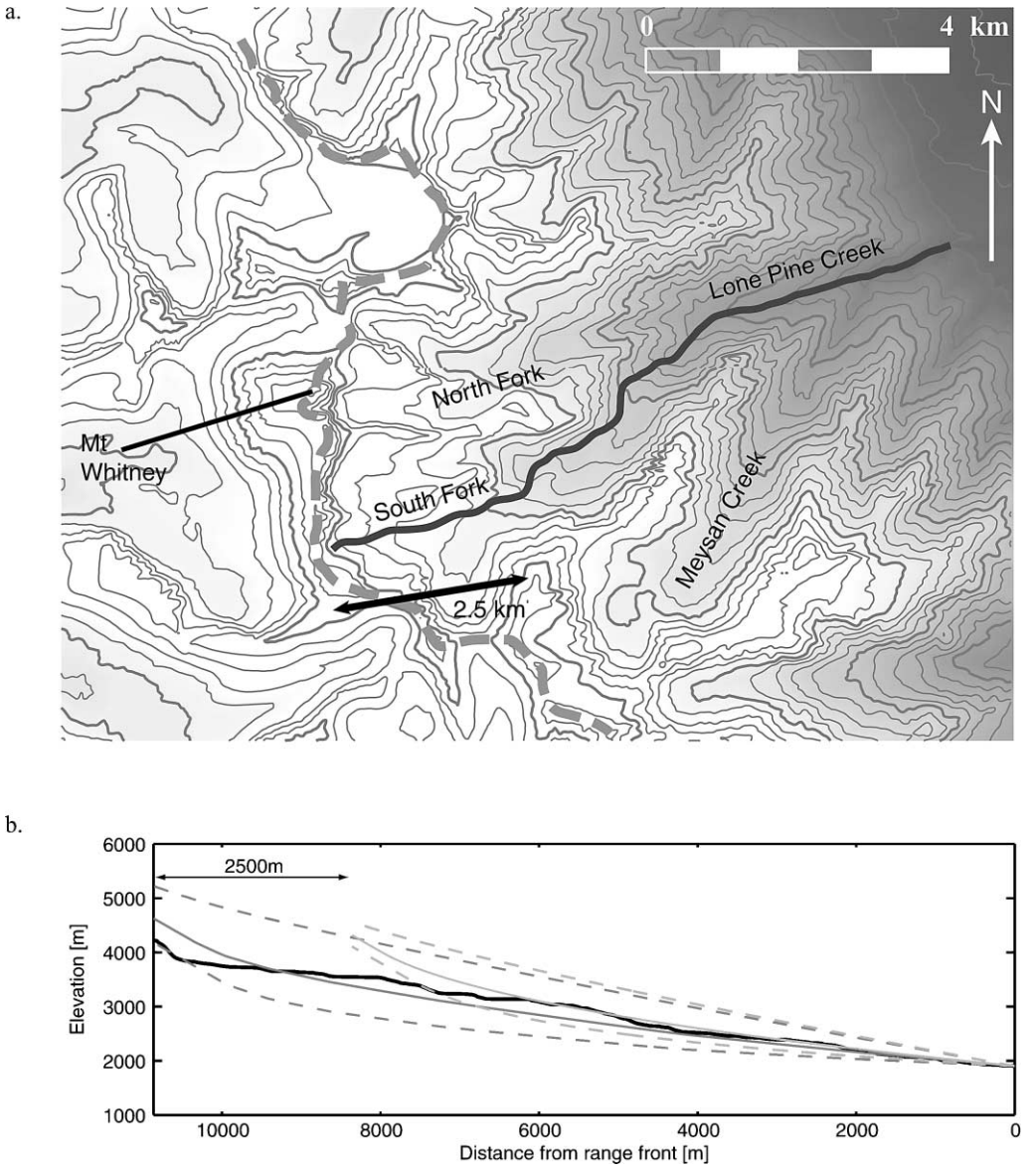


Fig. 12. Simulating headwall erosion in the south fork of Lone Pine Creek. (a) Contour map of the Lone Pine Creek basin. Notice the significant westward step in the divide at the head of Lone Pine Creek, passing just to the east of the summit of Mt Whitney. (b) Observed and simulated longitudinal profiles for Lone Pine Creek (present topography—black; full-length simulation—dark grey; shortened simulation—pale grey; simulated longitudinal profiles varying concavity and steepness by $\pm 1\sigma$—dashed). Estimated headwall erosion: 2500 m.

simulated profiles in the lower part of the basin. The headwall erosion represented in this way is the extra erosion beyond that which would have taken place in the fluvial system (i.e., we underestimate the total headwall erosion). We used Hack's Law parameters (Hack, 1957) to construct smaller basins of the same shape. For our purposes, Hack's Law can be written

$$A = k_h x^h \quad (4)$$

where $A$ is drainage area, $x$ is downstream distance along the longitudinal profile, and $k_h$ and $h$ are what we define as the Hack's Law constant and exponent, respectively. The constant and exponent were determined for each basin by regression analysis. We shortened the simulated drainage basins from the headwall end until the resulting longitudinal profile no longer undercut the present topography. In practice, this resulted in a fluvial profile that consistently matched the current topography up to ~3200 m, a little below the mean Quaternary ELA. The shorter profiles also reduce the amount of downcutting that is required in the upper part of the basin to move from the simulated nonglacial profile to the current profile, although the headwall erosion would still represent significant mass removal. Given the many unknowns in bedrock channel evolution and the uncertainty in our simulations of "expected" modern fluvial landforms, this argument for headwall erosion alone is perhaps unconvincing. However, the inferred amounts of headwall erosion are consistent with independent, if qualitative, field evidence for likely amounts of drainage divide retreat. For example, we suggest that the glacier in Birch Creek (Fig. 9b) has only cut headward ~100 m more than would have occurred under fluvial erosion, and we propose that this is because of competition with the south fork of Big Pine Creek, which lies at its head (Fig. 11a). Instead of divide

Table 2
Summary of divide migration results

| Basin | Degree of glaciation | Headward migration (m) | Rate (mm/year) |
|---|---|---|---|
| Alabama | None | 0 | 0 |
| Black | None | 0 | 0 |
| Inyo | None | 0 | 0 |
| Pinyon | None | 0 | 0 |
| South Fork, Lubken | None | 0 | 0 |
| Symmes | None | 0 | 0 |
| Diaz | Minor | 2500 | 1.25 |
| Division | Minor | 1500 | 0.75 |
| Thibaut | Minor | 400 | 0.20 |
| Bairs | Moderate | 550 | 0.28 |
| Goodale | Moderate | 2000 | 1.00 |
| Hogback | Moderate | 1400 | 0.70 |
| North Fork, Bairs | Moderate | 700 | 0.35 |
| North Fork, Lubken | Moderate | 1450 | 0.73 |
| Red Mountain | Moderate | 750 | 0.38 |
| Armstrong | Significant | 1000 | 0.50 |
| George | Significant | 850 | 0.43 |
| North Fork, Oak | Significant | 1200 | 0.60 |
| Sardine | Significant | 1400 | 0.70 |
| Sawmill | Significant | 3000 | 1.50 |
| Shepherd | Significant | 700 | 0.35 |
| Taboose | Significant | 900 | 0.45 |
| Tuttle | Significant | 1200 | 0.60 |
| Birch | Full | 100 | 0.05 |
| Independence | Full | 100 | 0.05 |
| Lone Pine | Full | 2500 | 1.25 |
| South Fork, Oak | Full | 2650 | 1.33 |
| Tinemaha | Full | 2150 | 1.08 |

migration, the combined action of these two glaciers has been to carve the horn known as The Thumb. The adjacent basin to the south, Tinemaha Creek (Figs. 9c and 11a), has cut a large "bite" out of the divide, which deviates noticeably to the west at its head. Here we require ~2150 m of "extra" headwall erosion to obtain a good fit between the simulated and observed profiles below ~3200 m (Fig. 11c). This headward cutting corresponds to an arguably reasonable rate of ~1.1 mm/year faster than the fluvial rate over the Quaternary (~2 Ma). The south fork of Lone Pine Creek, below Mt. Whitney, demonstrates a similar story (Fig. 12). Here, our best fit between the simulated profile and the observed glacial profile below ~3200 m requires shortening the simulated profile by ~2500 m (Fig. 12a). This again is consistent with the deviation of the divide around the head of the basin (Fig. 12b).

We also obtained a consistent story looking at the tributaries in selected basins. Fig. 11 illustrates our inferred variation in amounts of relative headwall erosion for three tributaries of Tinemaha Creek. Our method suggests that Tinemaha Creek is being enlarged in all directions, but is growing most rapidly at the range crest (profiles 2; Fig. 11c), lengthening the basin, rather than at the tops of its smaller tributaries (e.g., profile 3: Fig. 11d). This is consistent with what one might suggest from the basin morphology, as the head of the basin has a quite angular form with the "fastest growing" tributary at its apex, as opposed to a more typical morphology with a rounded head to the basin. Profile 1 (Fig. 11b) is essentially a nonglacial chute, so the fact that we attribute ~500 m of glacial headwall erosion to this profile illustrates the imperfect nature of the technique.

Table 2 summarises best-fit amounts of headwall erosion for each of our basins. The calculated headwall erosion rates are lower bounds on absolute headwall erosion rates because of the unknown headwall erosion rate that would have been taking place under the nonglacial regime, but they fall within the range of previously reported rockwall erosion rates in Alpine settings (Table 3). There is no correlation between degree of glaciation and rate of headwall erosion. Instead, local setting appears to be the major control on headwall erosion rate. We suggest that the slow headwall erosion in Shepherd and Independence Creeks is due not to competition, as in Birch Creek, but to the occurrence of transfluent ice at the head of the basin. We anticipate that an ice cap straddling the divide will act to protect the headwall, with relatively stagnant ice causing minor abrasion and insulating against freeze–thaw processes, and the lack of a bergschrund preventing water from reaching the glacier bed. Further studies of the mechanics of, and controls on, headward erosion by alpine glaciers are warranted.

## 6. Discussion

We have observed increasing relief with greater degree of glaciation in the basins of the eastern Sierra Nevada, but attribute this principally to the larger size of these basins. The amount of relief production that

Table 3
Published rockwall retreat rates for Alpine settings

| Location | Lithology | Rockwall retreat rate (mm/year) | | | Source |
|---|---|---|---|---|---|
| | | min | mean | max | |
| *Alpine environments, present day* | | | | | |
| Tatra Mountains | Dolomite | 0.1 | | 3.0 | Kotarba, 1972 |
| Front Range | Various | | 0.76 | | Caine, 1974 |
| French Alps | Various | 0.05 | | 3.0 | Francou, 1988 |
| Japanese Alps | Sandstone and shale | 0.03 | 0.1 | 0.3 | Matsuoaka and Sakai, 1999 |
| *Alpine environments, Holocene* | | | | | |
| Swiss Alps | Various | 1.0 | | 2.5 | Barsch, 1977 |
| Austrian Alps | Gneiss, schist | 0.7 | | 1.0 | Poser, 1954 |

can be ascribed to the onset of glacial erosion is not tightly constrained, but is probably small. Given a prior, well-dissected fluvial landscape, relief will only be produced by glacial erosion through its ability to erode headward into a low-relief surface at a more rapid rate than the fluvial system, enlarging drainage basins. This will be important in the special case of erosion into a plateau surface. As a simple illustration, consider the limiting case of headward erosion into a very low-relief plateau surface. Suppose that the basin of interest has $h$=1.6 and $k_h$=5 (Eq. (4)) and begins the Quaternary with a length of 9 km, yielding a drainage area of $\sim 10^7$ m$^2$. This would result in a mean geophysical relief (from Fig. 7) of $\sim$200 m. Suppose an equivalent area with very low relief lies "upstream" of this, giving a mean geophysical relief of $\sim$100 m across the region as a whole. Now suppose that the basin is enlarged during the Quaternary by glacial headward erosion to cover the whole of the $2\times10^7$ m$^2$ area, corresponding to lengthening by $\sim$4.5 km or headward erosion at a rapid rate a little above 2 mm/year. From Fig. 7 again, this basin will now have a mean geophysical relief of $\sim$250 m, so that overall the region will have seen an increase in geophysical relief of only $\sim$150 m. This corresponds to a maximum isostatic response of $\sim$123 m. In general, while we suspect that glaciers could well erode headward at a faster rate than rivers, thus still being an agent of relief production, the difference is probably insufficient to have a major effect on mean relief and hence isostatic response. Instead, we find that in comparing simulated modern fluvial topography with observed glaciated topography, the major impact of glacial erosion during the Quaternary has been a substantial lowering of peaks, ridgelines, and valley floors high in the range (above $\sim$3200 m) and thus a major reduction of trunk stream relief. This substantial lowering suggests that at the elevations at which they have been present for the greatest portion of the Quaternary (Porter, 1989), glaciers are capable of eroding at faster rates than rivers, lowering the peaks at a faster rate than the isostatic uplift that they might induce.

We have demonstrated that enhanced glacial erosion was concentrated in a narrow band along the crest of the range (elevations $>$3200 m). Some glaciers have apparently cut predominantly downward and brought ridgelines down with them, while other glaciers have cut mostly in a horizontal, headward direction with less impact on ridgeline elevations. At present, the Sierra Nevada crest is at a quite uniform elevation throughout the study area. We speculate that, prior to glaciation, the range could well have had a more undulatory crest. As shown by Small and Anderson (1995), the combined effects of erosion at the range crest and deposition in the Great Valley to the west can lead to significant flexural–isostatic tilting of the Sierra Nevada block. If the Sierra Nevada block is modelled as a broken (along the eastern scarp) elastic plate, such erosional redistribution of mass may be sufficient to explain a significant fraction of the observed tilt of Miocene lava beds (e.g., Huber, 1981). If this effect has been significant during the Quaternary, the induced acceleration in relative baselevel fall on streams draining the eastern Sierra Nevada could potentially have steepened the river valleys and would be incorporated into our simulations of modern nonglacial topography. Full consideration of the possible implications would require analysis of the topography of the much larger western drainages and flexural–isostatic modelling of the Sierra Nevada block as a whole—an analysis beyond the scope of the present study. Our analysis instead focussed on the more general problem of relief evolution in adjacent glaciated and unglaciated drainage basins that have experienced the same tectonic history.

Our general conclusions are probably valid for other temperate mountain ranges in low-moderate uplift rate settings. In colder regions, glacial ice could be frozen to the bed, drastically reducing erosion rates (Braun et al., 1999; Cuffey et al., 2000) and permitting higher peak elevations (Whipple et al., 1999). It is not clear whether the glacial erosion system will behave differently in a rapidly uplifting mountain range, where glacial erosion might not keep pace with uplift, or the glaciers might at least have to steepen (analogous to the reaction of the fluvial system) to do so. We envision a number of competing factors. Glacier beds at high elevations are more likely to be at subfreezing temperatures, reducing erosion rates (Cuffey et al., 2000). However, these high elevations could also interrupt airflow, causing increased orographic precipitation, which at higher altitudes would also fall as snow year round, thus contributing to increased glaciation (as suggested by

Molnar and England, 1990). We note that the region around Nanga Parbat exhibits spectacular hillslopes sometimes covering a 3-km range in elevation. There are no hillslopes approaching this scale in the Sierra Nevada, and we hesitate to speculate on their likely impact on the relief structure or even on why such enormous steep slopes are able to develop. These slopes could cause greater snow avalanching, hindering development of glaciers on the slopes themselves, but at the same time this avalanching would contribute significant volumes of snow and ice to the glaciers at the base of the slopes, enhancing mass balance and erosion. If glacial erosion is not coupled effectively with hillslope erosion there would be a high potential for relief production. Avalanching would also bring rock debris onto the glacier surface, shielding it from ablation and further enhancing erosion. Recent authors have emphasised the potential importance of subglacial water in erosion processes (e.g., Alley et al., 1999), but we cannot speculate about the consequences of variations in the subglacial hydrology between the Sierra Nevada and other settings. At present, neither the importance of subglacial hydrology to erosion nor the response of the hydrological system to steepening are well constrained. Thus, we feel it would be unwise to extrapolate our results too far; further study in other settings is needed.

How might the topographic distinctions that we have found in the Sierra Nevada be attributable to factors other than the glaciation history? One of the most beneficial features of the eastern Sierra Nevada as the field site for this study was the relatively simple and uniform tectonic history. The major lithologic variation lies in the nature of jointing within the Cretaceous granites. Our reconnaissance field studies indicate that just a few valleys exhibit greater than average joint density and that the consequence of this is principally a greater volume of colluvium in the valley (e.g., Armstrong Canyon) to offset the steeper valley walls. Thus, no net effect on the estimation of relief from the DEM is noted. The nonglaciated basins are all shorter than their glaciated counterparts, so that their heads lie farther into the rain shadow generated by this mountain range. Possibly, fluvial basins sourced higher in the range with a greater discharge and higher erosivity would have reduced concavity and steepness in comparison with the current, shorter nonglaciated basins (Whipple et al., 1999) and hence be more similar in form to the current glaciated profiles. We believe that this would be a minor effect. The nonglaciated basins that we have studied have a considerable range in drainage area, but very consistent concavities and steepnesses (e.g., Alabama vs. Symmes Creeks). Such a pattern of shallower, larger fluvial basins would also be inconsistent with our observation that the lower parts of our glaciated profiles match very closely the simulated fluvial profiles using the steepness ($k_s$) and concavity ($\theta$) of the modern nonglaciated basins.

## 7. Conclusions

We have demonstrated that glacial erosion is responsible for redistribution of relief, producing relief high in the drainage basin in the cirques, but resulting in lower relief where different tributaries converge. In the absence of a change in basin size, the net effect is to retain the same overall geophysical relief, so while glacial erosion mechanisms that both enhance and reduce relief have been active in the eastern Sierra Nevada, neither has been dominant. Glaciers have been responsible for bringing down both valley floors and ridgelines, suggesting that glaciers are capable of eroding at faster rates than rivers in this environment and that the glacial and hillslope systems are closely coupled. Whereas the glaciated basins in the eastern Sierra are associated with higher relief in comparison with their fluvial neighbours, this is principally due to basin size: the fluvial simulations based on the drainage networks of the glacial basins have geophysical relief similar to the current topography. Our preliminary attempts to evaluate the relative amounts of headward erosion in the fluvial and glacial systems suggest that, while local effects are very important, these headward erosion rates are generally higher in the glacial system. This leads to the possibility of enhanced relief production if this erosion cuts into a low relief surface, but the effect is likely to be small.

Our analyses indicate that the case for ridgeline uplift through isostatic response to enhanced valley erosion put forward by Molnar and England (1990) is exaggerated, at least for the Sierra Nevada. We note, however, that enhanced rates of erosion in the glacial

system will produce rugged topography and large volumes of sediment, both of which could be interpreted as reflecting relief production and misconstrued as evidence of accelerated late Cenozoic tectonism, as argued by Molnar and England (1990). At the same time, our results suggest that there will be a major negative feedback in the system proposed by Raymo and Ruddiman (1992) in that, whereas erosion rates may rise as a result of uplift and subsequent global cooling, the development of the glacial system will ultimately limit ridgeline elevations and relief. To return to the questions posed in the introduction, we find that, in the Sierra Nevada, glacial erosion is capable of reducing ridgeline elevations, but does not significantly enhance relief unless it enlarges a drainage basin into low-relief topography. However, the focussed glacial erosion above the ELA could contribute to far-field flexural–isostatic effects. We have identified the following areas for future research: (i) mechanisms, rates, and controls on headwall erosion in both the fluvial and glacial systems; (ii) the role of glacial erosion in areas of extreme tectonic activity; and (iii) limits to cirque headwall relief.

## Acknowledgements

We would like to take this opportunity to thank Greg Tucker, Eric Leonard, Noah Snyder, and Eric Kirby for the many valuable discussions, Ryan Ewing for the long-suffering field assistance, and Noah Snyder, Julia Baldwin and Marin Clark for the helpful comments on early versions of this manuscript. The comments of an anonymous reviewer greatly improved the clarity and thoroughness of the manuscript. This work was supported by NSF grants EAR-9980465 and EAR-9725723 (to KXW), a NASA Graduate Fellowship (to SHB), a NASA GSFC Graduate Student Research Grant, and a GSA Fahnestock Award (to SHB).

## References

Ahnert, F., 1984. Local relief and the height limits of mountain ranges. Am. J. Sci. 284 (9), 1035–1055.

Alley, R.B., Strasser, J.C., Lawson, D.E., Evenson, E.B., Larson, G.J., 1999. Glaciological and geological implications of basal-ice accretion in overdeepenings. In: Mickelson, D.M., Attig, J.W. (Eds.), Glacial Processes Past and Present. Geological Society of America Special Paper, vol. 337, pp. 1–9, Boulder, CO.

Barsch, D., 1977. Eine Abschälung von Schuttproduktion und Schutttransport im Bereich aktiver Blockgletscher der Schweizer Alpen. Z. Geomorphol., Suppl. 28, 148–160.

Bateman, P.C., 1965. Geology and tungsten mineralization of the Bishop District, California. U.S. Geol. Surv. Prof. Pap. 470, 208 pp.

Beaumont, C., Fullsack, P., Hamilton, J., 1992. Erosional control of active compressional orogens. In: McClay, K.R. (Ed.), Thrust Tectonics. Chapman & Hall, London, pp. 1–18.

Boulton, G.S., 1974. Processes and patterns of glacial erosion. In: Coates, D.R. (Ed.), Glacial Geomorphology. George Allen & Unwin, London, pp. 41–87.

Braun, J., Zwartz, D., Tomkin, J., 1999. A new surface-processes model combining glacial and fluvial erosion. Ann. Glaciol. 28, 282–290.

Brocklehurst, S.H., Whipple, K.X., 1999. Relief production on the eastern side of the Sierra Nevada, California. Am. Geophys. Union, Trans. 80 (46), F442.

Brocklehurst, S.H., Whipple, K.X., 2000. Hypsometry of glaciated landscapes in the western U.S. and New Zealand. Am. Geophys. Union, Trans. 81 (48), F504.

Brozović, N., Burbank, D.W., Meigs, A.J., 1997. Climatic limits on landscape development in the northwestern Himalaya. Science 276, 571–574.

Burbank, D.W., 1991. Late Quaternary snowline reconstructions for the southern and central Sierra Nevada, California and a reassessment of the "Recess Peak Glaciation". Quat. Res. 36 (3), 294–306.

Caine, N., 1974. The geomorphic processes of the alpine environment. In: Ives, J.D., Barry, R.G. (Eds.), Arctic and Alpine Environments. Methuen, London, pp. 721–748.

Chamberlin, T.C., 1899. An attempt to frame a working hypothesis of the cause of glacial periods on an atmospheric basis. J. Geol. 7: 545–584, 667–685, 751–787.

Clark, D.H., Gillespie, A.R., 1997. Timing and significance of late-glacial and Holocene cirque glaciation in the Sierra Nevada, California. Quat. Int. 38–39, 21–38.

Clark, D.H., Clark, M.M., Gillespie, A.R., 1994. Debris-covered glaciers in the Sierra Nevada, California, and their implications for snowline reconstructions. Quat. Res. 41 (2), 139–153.

Cuffey, K.M., Conway, H., Gades, A.M., Hallet, B., Lorrain, R., Severinghaus, J.P., Steig, E.J., Vaughn, B., White, J.W.C., 2000. Entrainment at cold glacier beds. Geology 28 (4), 351–354.

Flint, J.J., 1974. Stream gradient as a function of order, magnitude, and discharge. Water Resour. Res. 10 (5), 969–973.

Francou, B., 1988. Talus formation in high mountain environments: Alps and tropical Andes. Doctoral Thesis, Université de Paris XVII, France.

Gilchrist, A.R., Summerfield, M.A., Cockburn, H.A.P., 1994. Landscape dissection, isostatic uplift, and the morphologic development of orogens. Geology 22 (11), 963–966.

Gillespie, A.R., 1982. Quaternary glaciation and tectonism in the southeastern Sierra Nevada, Inyo County, California. PhD Thesis, California Institute of Technology, Pasadena, 695 pp.

Hack, J.T., 1957. Studies of longitudinal stream profiles in Virginia and Maryland. U.S. Geol. Surv. Prof. Pap. 294-B, 97 pp.

Hallet, B., 1996. Glacial quarrying: a simple theoretical model. Ann. Glaciol. 22, 1–8.

Hallet, B., Hunter, L., Bogen, J., 1996. Rates of erosion and sediment evacuation by glaciers: a review of field data and their implications. Global Planet. Change 12 (1–4), 213–235.

Hallet, B., Merrand, Y., Koppes, M.N., Anders, A., 2000. Recent advances in the study of glacial erosion through field research and theory. GSA Abstr. Prog. 32 (7), A328.

Hicks, D.M., McSaveney, M.J., Chinn, T.J.H., 1990. Sedimentation in proglacial Ivory Lake, Southern Alps, New Zealand. Arct. Alp. Res. 22 (1), 26–42.

Hooke, R.L., 1991. Positive feedbacks associated with erosion of glacial cirques and overdeepenings. Geol. Soc. Am. Bull. 103 (8), 1104–1108.

Huber, N.K., 1981. Amount and timing of Late Cenozoic uplift and tilt of the Central Sierra Nevada, California—evidence from the Upper San Joaquin River. U.S. Geol. Surv. Prof. Pap. 1197, 28 pp.

Koons, P.O., 1989. The topographic evolution of collisional mountain belts: a numerical look at the Southern Alps, New Zealand. Am. J. Sci. 289 (9), 1041–1069.

Kotarba, A., 1972. Comparison of physical weathering and chemical denudation in the Polish Tatra Mountains. In: Macar, P., Pissart, A. (Eds.), Processus Périglaciaires Études sûr le Terrain. Université Liège, Liège, Belgium, pp. 205–216.

Leopold, L.B., Wolman, M.G., Miller, J.P., 1964. Fluvial Processes in Geomorphology. Freeman, San Francisco, CA, 522 pp.

MacGregor, K.C., Anderson, R.S., Anderson, S.P., Waddington, E.D., 2000. Numerical simulations of glacial valley longitudinal profile evolution. Geology 28 (11), 1031–1034.

Matsuoka, N., Sakai, H., 1999. Rockfall activity from an alpine cliff during thawing periods. Geomorphology 28 (3–4), 309–328.

Merrand, Y., Hallet, B., 2000. A physically based numerical model of orogen-scale glacial erosion: importance of subglacial hydrology and basal stress regime. GSA Abstr. Prog. 32 (7), A329.

Molnar, P., England, P., 1990. Late Cenozoic uplift of mountain ranges and global climate change: chicken or egg? Nature 346, 29–34.

Montgomery, D.R., 1994. Valley incision and the uplift of mountain peaks. J. Geophys. Res. 99 (B7), 13913–13921.

Montgomery, D.R., Foufoula-Georgiou, E., 1993. Channel network source representation using digital elevation models. Water Resour. Res. 29 (12), 3925–3934.

Moore, J.G., 1963. Geology of the Mount Pinchot Quadrangle, Southern Sierra Nevada, California. U.S. Geol. Surv. Bull. 1130, 152 pp.

Moore, J.G., 1981. Geologic map of the Mount Whitney Quadrangle, Inyo and Tulare Counties, California, GQ-1545. US Geological Survey Map.

Porter, S.C., 1989. Some geological implications of average Quaternary glacial conditions. Quat. Res. 32 (3), 245–261.

Poser, H., 1954. Die Periglazial-Ersheinungen in der Umgebung der Gletscher des Zemmgrundes (Zillentaler Alpen). Göttinger Geogr. Abh. 15, 125–180.

Raymo, M.E., Ruddiman, W.F., 1992. Tectonic forcing of late Cenozoic climate. Nature 359, 117–122.

Sklar, L., Dietrich, W.E., 1998. River longitudinal profiles and bedrock incision models: stream power and the influence of sediment supply. In: Tinkler, K.J., Wohl, E.E. (Eds.), Rivers Over Rock. Geophysical Monograph, American Geophysical Union, Washington, DC, pp. 237–260.

Small, E.E., Anderson, R.S., 1995. Geomorphically driven Late Cenozoic rock uplift in the Sierra Nevada, California. Science 270, 277–280.

Small, E.E., Anderson, R.S., 1998. Pleistocene relief production in Laramide mountain ranges, western United States. Geology 26 (2), 123–126.

Snyder, N.P., Whipple, K.X., Tucker, G.E., Merritts, D.J., 2000. Landscape response to tectonic forcing: DEM analysis of stream profiles in the Mendocino triple junction region, northern California. Geol. Soc. Am. Bull. 112 (8), 1250–1263.

Sugden, D.E., John, B.S., 1976. Glaciers and Landscape Arnold, London, 376 pp.

Tarboton, D.G., Bras, R.L., Rodriguez-Iturbe, I., 1991. On the extraction of channel networks from digital elevation data. Hydrol. Processes 5 (1), 81–100.

Tomkin, J.H., Braun, J., 2000. The effect of glaciation on relief in an active orogen: a numerical modelling study. Earth Planet. Sci. Lett. Am. Geophys. Union, Trans. 81 (48), F504.

Tucker, G.E., Bras, R.L., 1998. Hillslope processes, drainage density, and landscape morphology. Water Resour. Res. 34 (10), 2751–2764.

Tucker, G.E., Slingerland, R.L., 1994. Erosional dynamics, flexural isostasy, and long-lived escarpments: a numerical modeling study. J. Geophys. Res. 99 (B6), 12229–12243.

Tucker, G.E., Slingerland, R.L., 1997. Drainage basin responses to climate change. Water Resour. Res. 33 (8), 2031–2047.

Wager, L.R., 1933. The rise of the Himalayas. Nature 132, 28.

Weissel, J.K., Pratson, L.P., Malinverno, A., 1994. The length-scaling properties of topography. J. Geophys. Res. 99 (B7), 13997–14012.

Whipple, K.X., Tucker, G.E., 1999. Dynamics of the stream-power river incision model; implications for height limits of mountain ranges, landscape response timescales, and research needs. J. Geophys. Res. 104 (B8), 17661–17674.

Whipple, K.X., Kirby, E., Brocklehurst, S.H., 1999. Geomorphic limits to climate-induced increases in topographic relief. Nature 401, 39–43.

Willgoose, G., 1994. A statistic for testing the elevation characteristics of landscape simulation models. J. Geophys. Res. 99 (B7), 13987–13996.